

Measuring the Structure of Epitaxially Assembled Block Copolymer Domains with Soft X-ray Diffraction

Gila E. Stein,^{*,†,§} J. Alexander Liddle,[†] Andrew L. Aquila,[‡] and Eric M. Gullikson^{||}

[†]Center for Nanoscale Science and Technology, National Institute of Standards and Technology, Gaithersburg, Maryland 20899, [‡]Applied Science and Technology Graduate Group, University of California, Berkeley, California 94720, and ^{||}Materials Sciences Division, Lawrence Berkeley National Laboratory, Berkeley, California 94720. [§]Current address: Department of Chemical and Biomolecular Engineering, University of Houston.

Received August 28, 2009; Revised Manuscript Received October 26, 2009

ABSTRACT: The size, shape, and interface structure of poly(styrene-*b*-methyl methacrylate) block copolymer domains assembled on an epitaxial template are characterized with soft X-ray diffraction. The domain size and shape are deformed when the dimensions of the epitaxial template are incommensurate with the equilibrium dimensions of the block copolymer, producing sidewall angles in the range of 1–2° (±0.2°). The average width of the copolymer interface is (4.9 ± 0.1) nm. Comparison with mean-field theoretic predictions for the structure of block copolymer interfaces suggests a low-frequency variance in the copolymer interface position of 1.2 nm², or a low-frequency line-edge roughness of approximately 3 nm.

Introduction

The most sophisticated integrated circuits (ICs), such as microprocessors and memory chips, are patterned with optical lithography. The performance of semiconductor electronics is coupled to the resolution of the lithographic processes, and to keep pace with historic growth rates the dimensions of many circuit elements must shrink below 50 nm. This requires high-resolution imaging materials (resists) that offer precise control over feature size and density, low pattern roughness, and low defect concentrations over large areas.¹ It has been suggested that block copolymer self-assembly in tandem with optical lithography could satisfy these requirements.^{2,3} Block copolymers are constructed by linking together two (or more) chemically distinct homopolymer chains, and the immiscibility between the different segments drives them to self-assemble into periodic mesophases. The advantage is that thermodynamics determine the structure of the block copolymer resist, rather than the complex chemistry and exposure statistics associated with optical lithography, so the patterns can be highly uniform over large areas. Incorporating these systems into IC production is potentially very simple: The strategy proposed by Nealey et al. uses optical lithography to define a chemical template that directs the placement of each block copolymer domain with respect to the substrate (conceptually similar to epitaxial crystal growth).⁴ The self-assembly is speculated to “heal” errors in the chemical template, such as line width variations and pattern roughness.^{5,6} However, it is unclear how the shape of the block copolymer domains is deformed by the epitaxy process, or if the intrinsic roughness of the block copolymer interface is too large to be suitable for manufacturing. These questions are difficult to answer with scanning electron microscopy (SEM), which is the standard metrology tool for resist inspection, for the following reasons: First, SEM measurements are only sensitive to chemical contrast when operated at low voltages (~100 V), and under such conditions the resolution is limited to approximately 5 nm. Second, polymers are damaged during SEM imaging. The damage mechanisms and rates are

different for each block copolymer constituent, producing topography that introduces artifacts into the measurement. Third, a SEM measurement only samples approximately 1 μm², which is not statistically significant. Last, extracting accurate line widths or three-dimensional shapes from SEM data requires complex modeling to predict the image formation process.⁷

In this paper, we use transmission soft X-ray diffraction (SoXRD) to characterize the shape and intrinsic roughness of a lamellar poly(styrene-*b*-methylmethacrylate) (PS–PMMA) block copolymer resist assembled by epitaxy. The transmission diffraction geometry is illustrated in Figure 1. A single SoXRD measurement samples 500 μm × 300 μm, and is sensitive to the size, shape, periodicity, and roughness of the block copolymer domains. The scattering contrast at energies near the carbon absorption edge (≈280 eV) results from spatial variations in the types and densities of carbon chemical bonds,^{8–11} offering a highly sensitive probe of the block copolymer structure. Note that polymer nanostructures are typically characterized with transmission small-angle X-ray diffraction (SAXD), a technique that uses high energy X-rays (usually 8 keV) and diffraction angles in the range 2θ = 0.1–1°. A single SoXRD measurement covers diffraction angles in the range 2θ = 4–40°, which offers two advantages over SAXD: (1) sensitivity to three-dimensional domain shape and (2) increased separation between the first-order diffraction peak and low-*q* parasitic scattering.¹²

Electron beam lithography (EBL) was used to generate low-roughness chemical patterns comprised of hydrophobic/hydrophilic stripes on a *d* = 46 nm pitch, and the width of the hydrophobic stripe ranged from approximately 0.55*d* to 0.63*d*. This closely matches the equilibrium properties of the PS–PMMA resist, which has a lamellar periodicity of *L*₀ = (46 ± 1) nm and equal PS/PMMA domain sizes of (0.5 ± 0.02)*d*.¹³ The chemical patterns effectively directed the assembly of the PS–PMMA resist into defect-free gratings spanning 1 mm × 1 mm,¹⁴ where the PS and PMMA domains attach to the hydrophobic and hydrophilic stripes, respectively. An overview of this epitaxy process is shown in Figure 2, and details are provided in the Experimental Section. The structure of the chemical patterns cannot be directly measured with SoXRD due to poor scattering contrast,¹⁵ so we

*Corresponding author. E-mail: gstein@uh.edu.

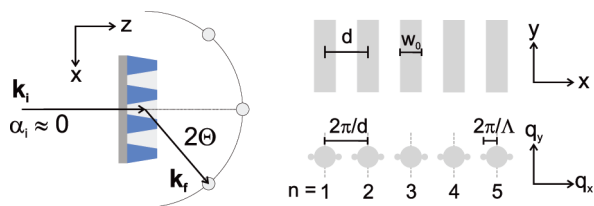


Figure 1. The transmission scattering geometry, along with an illustration of the grating parameters in real-space and a schematic of the diffraction peaks in reciprocal space. The primary diffraction peaks are situated at the nodes $n = 1, 2, \text{etc.}$, and satellite peaks are adjacent at $\pm 2\pi/\Lambda$. The satellite peaks result from noise during the electron-beam lithography exposure.¹⁶

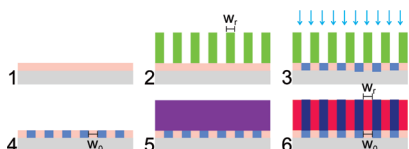


Figure 2. Overview of PS-PMMA assembly on chemical patterns. (1) Start with a hydrophobic PS surface. (2) Pattern with EBL (ZEP resist) and develop grating. (3) Oxidize to generate hydrophilic stripes. (4) Strip the ZEP resist. (5) Coat with PS-PMMA film. (6) Heat the film above the glass transition to order the PS-PMMA lamellae. The structures measured with SoXRD and SEM are depicted in steps 2 and 6.

instead characterize the EBL resist gratings that were used to generate the chemical patterns, and assume the line width and roughness are perfectly replicated (step 2 in Figure 2). The EBL resist gratings are denoted by the resist type “ZEP” throughout this manuscript.

This paper is organized as follows: First, a model for scattering from block copolymer gratings is presented that incorporates the domain shape, size, periodicity, and interfacial roughness. This model could be generalized to any type of resist, such as the photosensitive polymers used in optical lithography, offering a route to characterize resolution and line-edge roughness in the latent image. Second, the widths of the PS domains are calculated from SoXRD analysis and compared with SEM measurements. The domain widths measured by SoXRD are consistent with those predicted by strong-segregation theory for equal-volume block copolymers, while the dimensions measured by SEM are 30% to 40% larger and vary with magnification. Third, the sidewall angles of the PS domains are extracted from the SoXRD model and reported as a function of chemical pattern line width (i.e., the width of the hydrophobic stripes). The shapes of the PS-PMMA domains are deformed when the line width of the chemical pattern does not match the equilibrium domain size. Fourth, the average roughness of the PS-PMMA interface calculated from SoXRD and SEM measurements is reported. The SoXRD results agree with theoretical predictions for the structure of block copolymer interfaces, but the SEM data do not. The spatial frequency content of the block copolymer line-edge

roughness cannot be directly ascertained with SoXRD, but is estimated instead by comparing the experimental results with mean-field models for strongly segregated block copolymer interfaces. The low-frequency roughness is presumed to result from thermal fluctuations, and is consistent with a simple capillary wave model for polymer interfaces.

Model for X-ray Diffraction Analysis

Our objectives are to calculate the size, shape, and roughness of the block copolymer domains from the diffraction data. The diffracted intensity from a two-phase system with density profile $\rho(\mathbf{r})$ is as follows:

$$I(\mathbf{q}) = I_m(\mathbf{q}) + I_d(\mathbf{q}) = \langle |\rho(\mathbf{q})| \rangle^2 + \langle |\rho(\mathbf{q}) - \langle \rho(\mathbf{q}) \rangle| \rangle^2 \quad (1)$$

Note that $\rho(\mathbf{q})$ is the Fourier transform of $\rho(\mathbf{r})$. $I_m(\mathbf{q})$ is the scattering from the mean density profile, and reflects the average size, shape, pitch, and roughness of the gratings across the sampled area. $I_d(\mathbf{q})$ is the diffuse scattering from concentration defects or lattice disorder. In general, the diffuse scattering cannot be distinguished from background noise or parasitic scattering. However, we do detect weak satellite peaks in our data that result from *periodic* displacements in the grating pitch.¹⁶ These periodic displacements are the result of noise during the electron beam lithography, and are not associated with the self-assembly process. The following four sections outline a model for scattering from the block copolymer resist that is based on predictions for the structure of block copolymer interfaces in the strong segregation limit.^{17–19} We arrive at a form for $I(\mathbf{q})$ that can be applied to scattering from any type of resist, such as the chemically amplified photosensitive polymers that are typically used in optical lithography. Table 1 includes a list of notation and variables for analysis of SoXRD data.

Domain Shape. The average grating density profile $\rho(\mathbf{r})$ is modeled by convolving a one-dimensional lattice $\sum_n \delta_n(x - nd)$ with a shape function $s(\mathbf{r})$ that describes the line width $w_r(z)$ and sidewall angle $\phi(z)$ of the resist cross-section. The function $s(\mathbf{r})$ is equal to unity inside the boundaries of the shape and zero elsewhere. If the density transition across the phase boundary is perfectly sharp, the diffracted intensity is the product of the structure factor $\sum_n \delta_n(q_x - 2\pi n/d)$ with the form factor $|P(\mathbf{q})|^2$:

$$I_0(\mathbf{q}) = \sum_{n=-\infty}^{\infty} \delta(q_x - 2\pi n/d) |P(\mathbf{q})|^2 \quad (2)$$

$$P(\mathbf{q}) = \int_V s(\mathbf{r}) e^{-i\mathbf{q} \cdot \mathbf{r}} d\mathbf{v}$$

The form factor, or the shape of the resist cross-section, entirely determines the amplitude of the diffraction peaks, while the pitch (d) determines the peak positions. This simple

Table 1. Notation and Variables for Data Analysis

real space		Fourier space	
position vector	$\mathbf{r} = \{x, y, z\}$	scattering vector	$\mathbf{q} = \{q_x, q_y, q_z\}$
density function	$\rho(\mathbf{r})$	density function	$\rho(\mathbf{q})$
shape function	$s(\mathbf{r})$	form factor	$P(\mathbf{q})$
displacement wavelength	Λ	displacement frequency	$k_x = 2\pi/\Lambda$
Model Parameters			
grating pitch	d	fractional change in pitch	ε
apparent interface width	Δ_a	variance in edge position	$\langle \delta_x^2 \rangle$
standard deviation in edge position	σ	sidewall angle	$\phi(z)$
ZEP/BCP line width	$w_r(z)$	chemical pattern line width	w_0

model has been used to calculate the pitch and shape of larger ($d \sim 500$ nm) resist gratings measured by small-angle scattering.²⁰

The Structure of Block Copolymer Interfaces. The PS/PMMA interfaces are not perfectly sharp, but are characterized by a diffuse composition profile of finite width Δ . This is due to single-molecule displacements that produce a high frequency roughness. The diffuse interface is incorporated into the model by convolving the ideal density profile with a smoothing function $h(\mathbf{r})$ that describes the probability distribution of each phase across the interface.²¹ The composition of the PS phase across a PS/PMMA interface plane positioned at $x = 0$ is $\rho_{\text{PS}}(x) = 0.5[1 + \tanh(2x/\Delta)]$, so the appropriate smoothing function is $h_1(x, \Delta) = [\text{sech}^2(2x/\Delta)]/\Delta$.¹⁷ The diffracted intensity from the mean density profile is then as follows:

$$I_1(\mathbf{q}) = I_0(\mathbf{q})|H_1(\mathbf{q}, \Delta)|^2 \quad (3)$$

$$H_1(\mathbf{q}, \Delta) = (\pi\Delta q_x/4) \text{csch}(\pi\Delta q_x/4) \quad (4)$$

Comparing eqs 2 and 3, we see that broad interfaces produce a significant attenuation of the signal for $q_x > 2/\Delta$. The magnitude of the interfacial width, incorporating corrections for finite molecular weight, is calculated from the total degree of polymerization N , the Flory interaction parameter χ , and the statistical segment length a_{st} as follows:¹⁷

$$\Delta = \Delta_0[1 + 1.34/(\chi N)^{1/3}], \quad \Delta_0 = 2a_{\text{st}}\chi^{-0.5}/\sqrt{6} \quad (5)$$

Neutron reflectivity measurements from block copolymer interfaces have yielded interfacial widths that are larger than the value predicted by eq 5.²² This is attributed to thermal fluctuations that produce random shifts $\delta_x(y, z)$ in the position of the interface plane, which are the source of line-edge roughness in block copolymer resists. If the amplitudes of these fluctuations are small, i.e., $q_x\delta_x \ll 1$, then the scattering from the mean density profile is further attenuated by a factor $|H_2(\mathbf{q}, \delta_x)|^2 \cong (1 - q_x^2\langle\delta_x^2\rangle)$.^{19,23} The variance in the interface position $\langle\delta_x^2\rangle$ is estimated with a capillary wave model by integrating over the full distribution of fluctuations with upper and lower cut-offs of $q_{yz} \sim 1/\Delta$ and $q_{yz} \sim 1/d$, respectively. The interface tension from mean-field theory is $\gamma_0 = a_{\text{st}}\chi^{0.5}/(\nu 6^{1/2})$ where ν is the monomer volume.

$$\langle\delta_x^2\rangle = \frac{1}{2\pi\gamma_0} \ln\left(\frac{d}{\Delta}\right) \quad (6)$$

The functions H_1 and H_2 have similar forms over the experimental range $q_x \in [0, 1] \text{ nm}^{-1}$, so it is not feasible to extract Δ and $\langle\delta_x^2\rangle$ independently. Instead, we convolve the hyperbolic tangent concentration profile with a Gaussian distribution of interface positions.^{17,18} This fluctuation-broadened interface profile is well-modeled by a hyperbolic tangent function with an ‘‘apparent’’ width Δ_a :

$$\Delta_a^2 = \Delta^2 + 2\pi\langle\delta_x^2\rangle \quad (7)$$

The scattering from the mean density profile is then as follows:

$$I_2(\mathbf{q}) \cong I_0(\mathbf{q})|H_1(\mathbf{q}, \Delta_a)|^2 \quad (8)$$

The diffuse scattering from uncorrelated thermal fluctuations is too weak to accurately detect and fit to a model. However, including predictions for the magnitude of this component only changes the amplitude of the sixth order diffraction peak (the highest order observed) by $\sim 5\%$.¹⁹

Lattice Displacements. We observe satellite peaks in the experimental data that are located near the primary nodes at $q_{x,n} \pm k_x$, and the amplitudes of the satellites relative to the primary peaks scale as $I_{\text{sat}}/I_m \sim q_x^2$ (approximately). Such features are consistent with periodic compressions and extensions in the grating pitch, described by a displacement wave $\Delta\mathbf{x}_n = (\varepsilon/k_x) \cos(\mathbf{k} \cdot n\mathbf{d})$ with spatial frequency $|\mathbf{k}| = k_x = 2\pi/\Lambda$.²³ The grating pitch then varies sinusoidally from $d(1 - \varepsilon)$ to $d(1 + \varepsilon)$. If the amplitudes of the displacements are small, i.e., $\varepsilon \ll 1$, then the scattering from the mean density profile I_m and the diffuse scattering from the satellites $I_{\text{d,sat}}$ are

$$I_m(\mathbf{q}) = I_2(\mathbf{q})\{1 - q_x^2\varepsilon^2k_x^{-2}/4\} \quad (9)$$

$$I_{\text{d,sat}}(\mathbf{q}) = I_2(\mathbf{q} \pm \mathbf{k})\{q_x^2\varepsilon^2k_x^{-2}/4\} \quad (10)$$

The origin of these lattice displacements was determined to be noise during the electron beam lithography exposure, and a full discussion/analysis is reported elsewhere.¹⁶

SoXRD Data Analysis. The total diffracted intensity $I(\mathbf{q})$ from the block copolymer line gratings is calculated with eqs 1–10. The only component of this model that is specific to block copolymer resists is the form of the attenuation function described by eq 4, and it is straightforward to calculate a new attenuation function for a different probability distribution: For example, a step function interface profile convolved with a Gaussian distribution of interface positions may better describe the exposure statistics in traditional optical and electron beam resists. However, if we assume a step function profile for the mean-field block copolymer interface (instead of the hyperbolic tangent distribution), the magnitude of Δ_a recovered is within ~ 0.3 nm, demonstrating that the form of the interface function is not critical to the analysis. As such, both block copolymer and ZEP resist gratings are analyzed with an attenuation based on the hyperbolic tangent interface profile (eq 4).

The shape of the resist cross-section $s(\mathbf{r})$ and apparent interfacial width Δ_a were calculated for each sample by fitting the diffraction data to the model $I(\mathbf{q})$ convolved with an experimental resolution function.²⁴ The shape function $s(\mathbf{r})$ used for analysis of the PS–PMMA resist was a single trapezoid with the following adjustable parameters: trapezoid base (line width) $w_r(z = 0)$ and sidewall angle ϕ . The trapezoid height was constrained to 55 nm (the film thickness measured with a spectroscopic ellipsometer). The shape function $s(\mathbf{r})$ of the ZEP resist was approximated by a stack of two trapezoids with the following adjustable parameters: Base $w_r(z = 0)$, heights $H_{i=1,2}$, and sidewall angles $\phi_{i=1,2}$. The total height of the ZEP trapezoid stack was constrained to 33 nm (the film thickness measured by ellipsometry).

Results and Discussion

Representative scattering data from the PS–PMMA gratings assembled by epitaxy and the ZEP gratings prepared by EBL are shown in Figure 3a,b with the best-fit results. The intensity is scaled by a factor $q_x^2q_z^2$ to amplify the errors between raw data and fits. This scaling is selected because the form factor for a rectangular cross-section decays as $q_x^{-2}q_z^{-2}$. Representative SEM images of the PS–PMMA and ZEP gratings are presented in Figure 4a,b. The line widths and line-edge roughness calculated from SEM and SoXRD measurements are compared in the following discussion. While the focus of this paper is characterization of the PS–PMMA structure, the ZEP SEM and SoXRD data are presented for the following reasons: First, the ZEP line

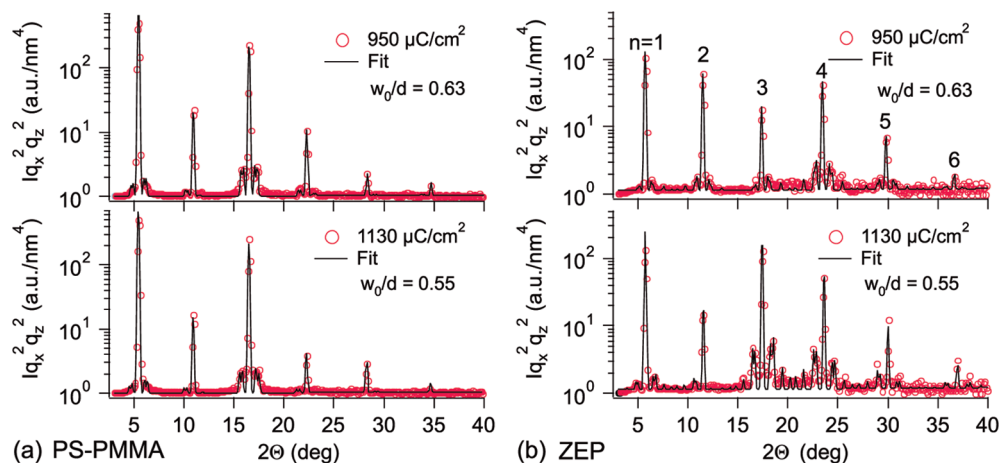


Figure 3. Diffraction data from the resist gratings, and fits to the model described by eqs 1–10: (a) PS–PMMA data and fit; (b) ZEP data and fit. The increase in EBL exposure dose is intended to vary the normalized line width w_0/d of the chemical patterns.

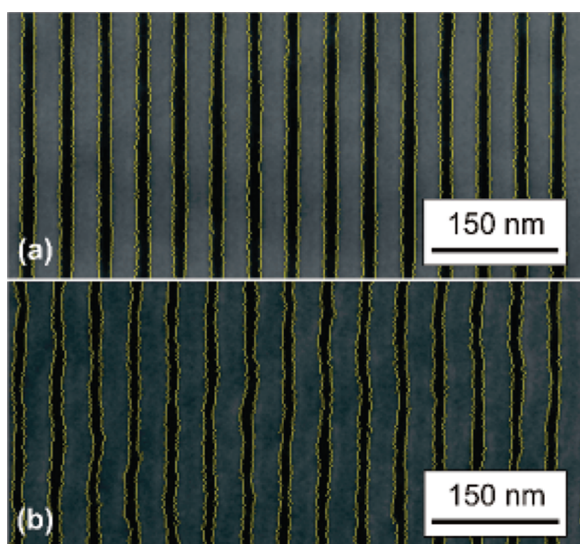


Figure 4. (a) SEM measurement of a ZEP grating produced by an EBL exposure dose of 950 $\mu\text{C}/\text{cm}^2$. (b) SEM measurement of a PS–PMMA grating assembled on chemical patterns generated with an EBL exposure dose of 950 $\mu\text{C}/\text{cm}^2$ ($w_0/d \approx 0.63$). The edge positions are marked in yellow.

widths are used to estimate the line widths of the chemical patterns (the epitaxial template). Second, ZEP line-edge roughness data are required to estimate the roughness of the chemical patterns. Third, the ZEP diffraction data serve as a control for characterizing the “satellite peaks,” which might otherwise be erroneously attributed to fluctuations in the block copolymer lattice.

Line Widths. The line widths w_r calculated from SoXRD and SEM measurements are reported as a function of EBL exposure dose in Figure 5a. SEM imaging is a complex process that involves the generation of both secondary and backscattered electrons having a distribution of energies. While the full resist volume is excited, the escape depth of the electrons is largely limited to the near surface region, and the signal from the sidewalls can vary as a function of both sidewall angle and roughness. In addition, beam-induced damage to the polymer components is unavoidable: The dominant mechanisms are cross-linking of the PS domains, and degradation of both PMMA and ZEP phases. Our analysis of the SEM data does not incorporate any modeling to describe these complex processes. Instead, we calculate the position of the resist edges from the maximum rate of change in the signal, and the SEM line width is simply the distance

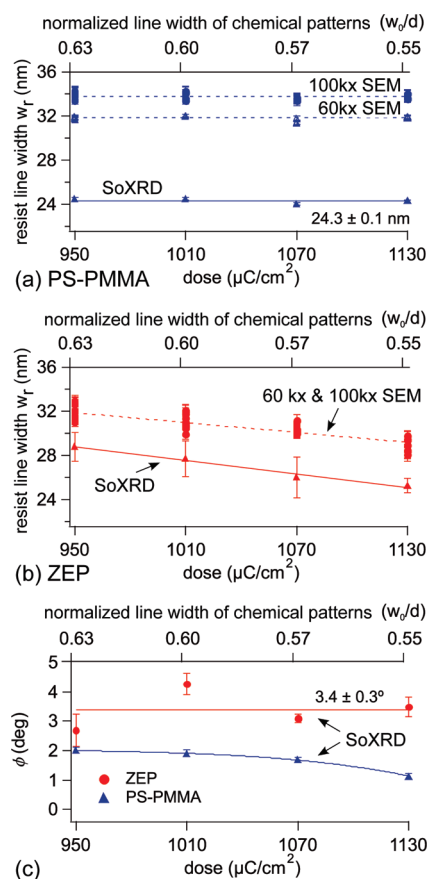


Figure 5. (a, b) Critical dimensions for PS–PMMA and ZEP as a function of EBL exposure dose, calculated from both SEM and SoXRD. The reported line width from SoXRD is the average through the film thickness. Note that the apparent dimension measured with SEM varies with magnification. (c) Average sidewall angles measured with SoXRD reported for ZEP and PS–PMMA. The blue curve through the PS–PMMA data set is a guide to the eye. Error bars on SEM measurements represent uncertainties calculated from interline statistics. Error bars on SoXRD data represent the uncertainty calculated from nonlinear regression analysis.

between adjacent edges. The SoXRD line widths reported for ZEP and PS–PMMA are the average through the film thickness. Four trends are clear: First, both the PS–PMMA and ZEP line widths calculated from SoXRD are systematically smaller than the corresponding SEM measurements.

This is not surprising since the secondary electron yield from the sidewalls is larger than the top surface, increasing the apparent line width of the resist gratings in SEM measurements. Second, the ZEP line width decreases linearly with EBL exposure dose according to both metrologies. On the basis of the SoXRD data, we estimate an 8% decrease in the normalized line widths of the chemical patterns from $w_0/d = 0.63$ to 0.55 (± 0.03) as the exposure dose increases from 950 to $1130 \mu\text{m}^2/\text{cm}^2$. Note that $w_0/d = 0.5 \pm 0.01$ is required to match the line width of the epitaxial template with the block copolymer domain width. Third, the average PS–PMMA line width is independent of EBL exposure dose/chemical pattern line width by either metrology. The predicted line width for an equal-volume lamellar structure with an equilibrium periodicity of $L_0 = (46 \pm 1) \text{ nm}$ is $(23 \pm 0.5) \text{ nm}$, and the value extracted from SoXRD is $(24.3 \pm 0.2) \text{ nm}$. This slight increase in line width may be induced by the epitaxial template. Fourth, the apparent PS–PMMA line width measured by SEM increases with increasing magnification. Higher SEM magnifications deposit more energy per unit area into the film, so there is more damage to the PMMA phase. It is likely that the PMMA domains shrink to expose the PS edges, which increases the secondary electron yield from the edges. We draw two important conclusions from the data: (1) The SEM data capture the qualitative trends, but are not accurate; (2) the PS–PMMA self-assembly does offer predictable control over the feature dimensions.

Sidewall Angles. The sidewall angles for ZEP and PS–PMMA gratings measured with SoXRD are reported in Figure 5b. The sidewall angle for the ZEP gratings, averaged through the grating thickness, is in the range $\phi = 3\text{--}4^\circ$ for all doses. This is consistent with SEM measurements of the resist cross-section (see Experimental Section and Figure 8). The shape of the PS phase in the PS–PMMA gratings is deformed by the epitaxy process: The average PS sidewall angle decreases from $\phi = (2.0 \pm 0.1^\circ)$ to $(1.1 \pm 0.1^\circ)$ as the normalized line width w_0/d decreases from approximately 0.63 to 0.55 (± 0.05). These angles are consistent with mean-field simulations of the domain shape as a function of chemical pattern line width.⁵ For manufacturing, the sidewall angles should (ideally) be zero across the substrate.

Interface Width and Line-Edge Roughness. It is useful to consider predictions for the structure of a PS–PMMA interface when evaluating our experimental results. The mean-field interfacial width for PS–PMMA at 240°C is $\Delta \approx 4.0 \text{ nm}$ (eq 5). The variance in the interface position predicted by the capillary wave model is $\langle \delta_x^2 \rangle \approx 1.2 \text{ nm}^2$ (eq 6), producing an apparent interfacial width of $\Delta_a \approx 4.9 \text{ nm}$ (eq 7). The following physical parameters were used for these calculations: $\chi \approx 0.037$,²⁵ $a_{\text{st}} \approx 0.68 \text{ nm}$,^{26–28} $\nu = 0.17 \text{ nm}^3$,^{26,29,30} and $N = 1015$. (Note that the value of χ selected for calculations is based on small-angle X-ray scattering data from nondeuterated PS–PMMA block copolymer,²⁵ and not the cloud point measurements from PS/PMMA blends reported by Callaghan et al.³¹ The Appendix to this article includes a comparison of the two χ values.) These predictions for interfacial structure are related to the conventional definitions of line-edge roughness as follows:

- The mean-field interface has a high-frequency line-edge roughness of approximately $3\sigma_{\text{HF}} = 3(\Delta^2/8)^{0.5} \approx 4.3 \text{ nm}$ for spatial frequencies greater than $1/\Delta = 200 \mu\text{m}^{-1}$.³² The SEM measurements cannot detect roughness at spatial frequencies greater than about $300 \mu\text{m}^{-1}$ (limited by low-pass filtering required for image processing, and 1.1 nm SEM pixel size).
- The fluctuation model predicts a low-frequency line-edge roughness of $3\sigma_{\text{LF}} = 3\langle \delta_x^2 \rangle^{0.5} = 3.3 \text{ nm}$ for

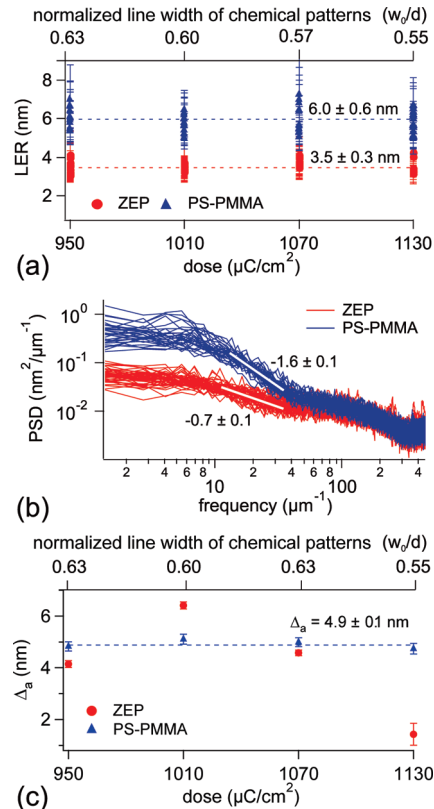


Figure 6. (a) ZEP and PS–PMMA line-edge roughness (LER = 3σ) calculated from SEM measurements. Error bars represent uncertainties calculated from interline statistics. (b) Power spectral density of the resist LER. Each curve corresponds with an individual image. Data exhibit a powerlaw decay over spatial frequencies of $6\text{--}40 \mu\text{m}^{-1}$. (c) Apparent interfacial width Δ_a measured from soft X-ray diffraction. (± 1 standard deviation). Error bars represent the uncertainty calculated from nonlinear regression analysis.

spatial frequencies in the range $1/d = 20 \mu\text{m}^{-1}$ to $1/\Delta = 200 \mu\text{m}^{-1}$. These spatial frequencies can be detected by our SEM imaging protocol.

The line-edge roughness (LER) of ZEP and PS–PMMA gratings calculated from SEM image analysis are shown as a function of EBL exposure dose in Figure 6a,b. LER is defined as 3σ , where σ is the standard deviation in the edge position, and the error bars represent uncertainties calculated from interline statistics. The average LER for ZEP and PS–PMMA are $(3.5 \pm 0.3) \text{ nm}$ and $(6.0 \pm 0.6) \text{ nm}$, respectively, and are independent of exposure dose and SEM magnification. The corresponding LER power spectra are presented in Figure 6b, and these data suggest that low-frequency ($\leq 40 \mu\text{m}^{-1}$) fluctuations are responsible for increased LER in block copolymers relative to ZEP. The power spectral density exhibits a power-law decay over the range of spatial frequencies $6 \mu\text{m}^{-1}$ to $40 \mu\text{m}^{-1}$, with decay exponents of $\eta = -0.7 \pm 0.1$ for ZEP and $\eta = -1.6 \pm 0.1$ for PS–PMMA. (Note that the capillary wave model for fluid interfaces described by eq 6 predicts $\eta = -2$.) The ZEP resist grating is used to generate the chemical patterns for epitaxy, so the PS–PMMA LER appears to be larger than that of the underlying template, indicating that it is an intrinsic property.

The apparent interfacial widths Δ_a for PS–PMMA and ZEP calculated from SoXRD analysis are reported in Figure 6c. These values reflect both high and low frequency roughness as described by eqs 7 and 8. Measurements of Δ_a for ZEP range between 4 and 6 nm at lower doses, and drop

to 1.5 nm at the highest dose. Since this trend is not observed in the SEM data, we believe the diffraction model described by eqs 1–10 does not accurately predict the scattering from ZEP at large values of q_x . This failure is likely due to variations in the resist dimensions across the sampled area, which attenuates the signal in a similar manner as interfacial roughness.³³ Such polydispersity in feature size could result from nonuniform development of the resist at lower exposure doses.

The average measured value of Δ_a for PS–PMMA is (4.9 ± 0.1) nm, and is independent of exposure dose. This measurement is larger than predictions for the mean-field interfacial width that incorporate chain end effects ($\Delta = 4.0$ nm), and matches predictions for an interface broadened by capillary waves ($\Delta_a = 4.9$ nm). The consistency between theory and experiment suggest that the magnitude of low frequency line-edge roughness in this PS–PMMA system can be predicted by the simple capillary wave model of eq 6, and is approximately $3\sigma_{lf} = 3\langle\delta_x^2\rangle^{0.5} = 3.3$ nm. (Note that the capillary wave model employs upper and lower cut-offs of $q_{yz} \sim 1/\Delta$ and $q_{yz} \sim 1/d$, respectively, suggesting that fluctuations at a longer length scale than the block copolymer periodicity are suppressed.) The most important consideration involved with estimating $\langle\delta_x^2\rangle$ from measurements of Δ_a is the accuracy of the physical constants used to calculate Δ : A 5% error in the physical parameters introduces a 0.2 nm uncertainty in calculations of Δ , and the uncertainty in measurements of Δ_a is 0.1 nm (standard deviation), producing an uncertainty in 3σ of approximately 1.6 nm. Calculations based on different χ values are included in the Appendix. Alternatively, the total line-edge roughness (both low and high frequency contributions) can be estimated from SoXRD measurements without specifying physical constants, and is approximately $3\sigma \approx 3(\Delta_a^2/8)^{0.5} \approx (5.2 \pm 0.2)$ nm.³²

Clearly there is a discrepancy between the SEM and SoXRD LER measurements, and we believe the SEM measurement of $3\sigma = (6 \pm 0.6)$ nm is erroneous. Large amplitude fluctuations that could produce high values of LER have been reported for homopolymer interfaces,^{34,35} but cannot be supported in block copolymers unless they are correlated across multiple domains. Large amplitude, coherent fluctuations can be produced by mismatch between the pitch of the chemical pattern and the equilibrium PS–PMMA periodicity (uniaxial stress).^{36,37} However, the present system is commensurate, and we do not observe the characteristic satellite peaks in the diffraction data that would accompany this phenomenon.³⁸ Although we have not verified the cause of this discrepancy, it is potentially a result of the electron beam/specimen interaction in the SEM: The beam preferentially etches the PMMA in the diblock, which could create additional variations in line-edge position that are not intrinsic to the material. For example, the PS interface may distort or collapse as the PMMA phase shrinks.

Conclusions

We have presented a simple model for analysis of diffraction data from nanoscale resist gratings. The model accurately characterizes the structure of a poly(styrene-*b*-methyl methacrylate) (PS–PMMA) resist (23 nm half-pitch) assembled by epitaxy: The domain size, interface width, and line-edge roughness extracted all closely match theoretical predictions for strongly segregated block copolymers. We find that the shapes of the PS and PMMA phases are deformed when the equilibrium domain sizes are incommensurate with the line widths of the underlying epitaxial patterns, and mismatch as small in the range of 10–25% ($\pm 5\%$) produces sidewall angles of 1 – 2° . Our results suggest the intrinsic

line-edge roughness for this PS–PMMA resist is $3\sigma \approx 3$ nm, consistent with the magnitude predicted by capillary wave models for polymer interfaces. These values of ϕ and 3σ are slightly larger than those required for integrated circuit manufacturing at the 23 nm node.¹

Experimental Section

Certain materials and procedures are identified in this paper in order to specify the experimental procedure adequately. Such identification is not intended to imply recommendation or endorsement by the National Institute of Standards and Technology, nor is it intended to imply that the materials or procedures identified are the best available for the purpose.

Substrate Fabrication. Transmission SoXRD experiments require the substrate to be transparent, so we fabricate all samples on silicon nitride (SiN) membranes that are approximately 50% transparent to 280 eV radiation. A 100 nm thick film of low-stress (silicon rich) SiN is deposited on clean 100 silicon wafers using low-pressure chemical vapor deposition with the following parameters: 7.44×10^{-5} mol/s (100 sccm) dichlorosilane, 1.49×10^{-5} mol/s (20 sccm) ammonia, 33 Pa (250 mT), and 835 °C. The deposition rate is 6.9 nm/min, and the film stress is (170 ± 10) MPa tensile. The front side of each substrate is then patterned with gold “alignment marks” that are aligned with the crystallographic axes of the silicon wafer. These marks are used to define the position and orientation of the electron beam lithography patterns. The backside of each wafer is patterned with an array of “windows” where the SiN film is removed with a CHF₃ reactive ion etch. After all electron beam lithography and PS–PMMA self-assembly steps are complete, membranes are created in these windows by etching away the silicon with a 30 wt % potassium hydroxide solution (aqueous) at 40 °C for 2 days. The resulting membranes span 1 mm \times 1 mm. The membranes are etched last so the substrate thermal conductivity is uniform through all the spin-casting and annealing steps required to generate the ZEP and PS–PMMA gratings. Additional information is provided in the Supporting Information.

Electron Beam Lithography. Substrates were coated with a 33 nm thick film of poly(methylstyrene-*co*-chloromethyl acrylate) electron beam resist (ZEP, Zeon Chemicals) and then baked at 180 °C for 2 min. Line gratings were patterned with electron beam lithography using an accelerating voltage of 100 keV, beam current of 1.1 nA, and beam step size of 2 nm. The pitch of the line gratings was 46 nm with a line bias of -11 nm (6-pass lines). The exposure doses ranged from 950 to 1130 $\mu\text{C}/\text{cm}^2$ to vary the grating line width w_0 . The coherence length of the gratings is determined by the length of the beam deflection, which was set to 16 μm . This means that 62 gratings, each spanning 16 $\mu\text{m} \times 16 \mu\text{m}$, were stitched together to pattern the full 1 mm \times 1 mm area. The ZEP resist was developed in hexyl acetate at -6 °C for 40 s, followed by a 10 s rinse in isopropyl alcohol, and then drying with nitrogen. Note that all gratings are aligned with the crystallographic axes of the silicon substrate, which is necessary to ensure the sample is properly aligned with the beamline geometry for SoXRD measurements.

Block Copolymer Epitaxy. PS–PMMA lamellae were assembled on chemical patterns (alternating hydrophobic/hydrophilic stripes) following the methods of Nealey et al.³⁹ Hydroxy-terminated PS ($M_n = 6.4$ kg/mol, PDI = 1.07) was purchased from Polymer Source and used as received. A PS brush was prepared by grafting to the substrate from the melt (a 30 nm thick film) at 140 °C for 24 h under high vacuum (10^{-5} Pa/ 10^{-7} Torr). The excess PS was removed by sonication in toluene at 50 °C for 30 min. The control point for this process is the contact angle of water: If this value is not equal to 90° across the entire wafer, the PS grafting density is not sufficient to achieve defect-free epitaxy. In such instances the grafting process is repeated. The PS brush was patterned using the electron beam lithography process described above, then the hydrophilic stripes were

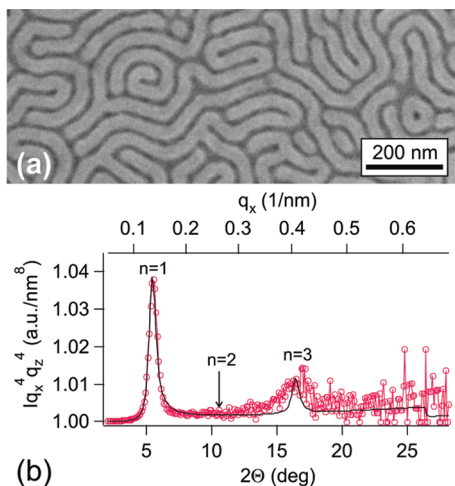


Figure 7. (a) SEM measurement of PS–PMMA lamellae on a neutral substrate. (b) Diffraction from PS–PMMA on a neutral substrate. The even diffraction orders are not visible because the PS and PMMA phases are of equal volume, and the domain walls are oriented perpendicular to the substrate.

generated with a 10 s reactive ion etch using 7.5×10^{-6} mol/s (10 sccm) O_2 at 1.6 Pa (12 mT), 10 W, and 60 V DC. The resist was then stripped in *n*-methyl pyrrolidone at 50 °C for 30 min, followed by sonication in toluene at 50 °C for 30 min. PS–PMMA films ($M_n = 100$ kg/mol, PDI = 1.12, 50% PS by volume) ranging in thickness from 40 to 55 nm were spun cast on the substrates, followed by annealing in air for 5 to 7 min at 240 °C. The equilibrium lamellar periodicity for this system is $L_0 = (46 \pm 1)$ nm, which is commensurate with the chemical patterns.

Equilibrium Properties for PS–PMMA. The equilibrium pitch and line width for the PS–PMMA lamellar block copolymer were determined with X-ray scattering from the “fingerprint” pattern shown in Figure 7a. This is the structure that results when a ~ 46 nm thick PS–PMMA film is cast on substrate coated with a “neutral” polymer brush,⁴⁰ then annealed in air at 240 °C for 5 min. The neutral polymer brush is a random copolymer of PS and PMMA ($M_n = 8.9$ kg/mol, PDI = 1.47, 59% PS, purchased from Polymer Source and used as received). This was prepared by grafting from the melt (a 30 nm thick film) while ramping the temperature from 140 to 250 °C over 24 h under high vacuum (10^{-5} Pa/ 10^{-7} Torr). The excess random copolymer was removed by sonication in toluene at 50 °C for 30 min. The contact angle of water on this neutral surface was 80°. From analysis of the scattering data shown in Figure 7b we determined the equilibrium pitch of the PS–PMMA domains is $d = (46 \pm 1)$ nm and the equilibrium line width is $w_0 = (0.5 \pm 0.02)$ (with $\phi = 0$). This confirms that the block copolymer equilibrium periodicity is commensurate with the pitch of the chemical patterns generated for epitaxy, and the $0.5d$ line width is expected for equal volume lamellar phases. The even-numbered diffraction orders are not visible in the fingerprint scattering patterns because these positions correspond with minima in the form factor (Figure 7b). However, both even and odd diffraction orders are observed in the PS–PMMA gratings (see Figure 3a), demonstrating that the domain shape is deformed by the epitaxy process.

Scanning Electron Microscopy. The PS–PMMA and ZEP samples were imaged with scanning electron microscopy (SEM) using a beam voltage of $E_2 = 1.5$ keV,⁴¹ a 2 mm working distance, a 30 μ m aperture, and magnifications of 60 $k\times$ and 100 $k\times$. The best resolution under these conditions is approximately 2 nm. The electron beam rapidly etches both PMMA and ZEP, so each area was measured for a maximum of 6 s. All images were stored in grayscale tiff format at a resolution of 1024 pixels/line. Data were filtered with a low-pass 5×5 median kernel, and

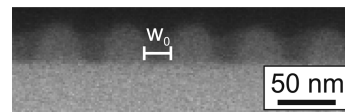


Figure 8. Cross-section of a ZEP grating measured by SEM.

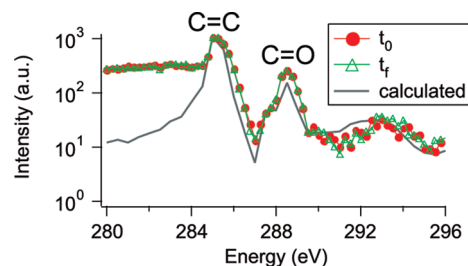


Figure 9. Representative contrast measurement from a PS–PMMA thin film before (t_0) and after (t_f) diffraction measurements. The peak at 285 eV corresponds with the aromatic pendant group in poly(styrene) (PS), and is used to normalize the data. The peak at 289 eV is associated with carbonyl groups in poly(methyl methacrylate) (PMMA). When exposed to high doses of radiation, PMMA undergoes chain scission, resulting in the destruction of carbonyl moieties.

then the edge positions of the resist lines were located from the maximum rate of change in the grayscale intensity. The average LER, average CD, and LER power spectrum were then calculated from the edge positions. Representative SEM measurements are shown in Figure 4 with the edge positions marked in yellow.

Cross sections of the ZEP and PS–PMMA gratings were prepared for SEM analysis by cleaving the silicon wafers at room temperature. The contrast from PS–PMMA was too low to image the structure without removing the PMMA phase, but an example of a ZEP cross-section is shown in Figure 8. These structures are difficult to image due to beam-induced etching, charging, and damage to the resist from sample preparation, but we do consistently observe sloped sidewalls.

X-ray Diffraction. Transmission soft X-ray diffraction (SoXRD) measurements were completed at the Advanced Light Source beamline 6.3.2 using photon energies of 270 eV ($\lambda = 4.59$ nm) for ZEP gratings and 284 eV ($\lambda = 4.37$ nm) for PS–PMMA gratings. The scattering geometry is illustrated in Figure 1. The sample is illuminated at normal incidence ($\alpha_i \approx 0$), and the scattering is recorded by scanning a channel electron multiplier detector mounted on a rotating arm from $2\theta = 2$ – 45° in 0.1° increments. The signal is averaged for 10 s per angle. Each diffraction measurement samples an area of $500 \mu\text{m} \times 300 \mu\text{m}$, and data were recorded from two locations per sample. The lateral coherence length of the radiation is on the order of a few micrometers. The resist grating axis was aligned to the y -axis with an accuracy of $\pm 1^\circ$. The elastic scattering vector is $\mathbf{q} = \mathbf{k}_f - \mathbf{k}_i$, where \mathbf{k}_i and \mathbf{k}_f are the incident and scattered wave vectors, respectively. Correcting for refraction at the polymer interfaces, the wave vectors inside the film are defined as $\mathbf{k}_i = 2\pi\{\sin \alpha_i, 0, (n_p^2 - \sin^2 \alpha_i)^{0.5}\}/\lambda$ and $\mathbf{k}_f = 2\pi\{\sin 2\theta, 0, (n_p^2 - \sin^2 2\theta)^{0.5}\}/\lambda$, where n_p is the refractive index of the polymer film. Polymers can be degraded or cross-linked by exposure to soft X-ray radiation, so testing for beam-induced chemistry changes was a critical component of the experiments. This was accomplished by measuring the scattering intensity (or PS–PMMA contrast) in transmission mode before and after each diffraction measurement. These “contrast” data are collected by fixing the detector angle at approximately 5° , which is the position of the first-order diffraction peak, and then collecting the intensity as a function of photon energy. An example of the resulting data is shown in Figure 9 and compared with the theoretical PS–PMMA contrast. The lack of change in 289 eV peak intensity indicates there is no detectable degradation of the PMMA phase. Contrast data below approximately 284 eV do not match the theoretical

Table 2. Fit Results for Analysis of SoXRD Data from Block Copolymer Line Gratings with Constrained $\phi = 0$ (i.e., a Rectangular Cross-Section)^a

w_0/d	w_r (nm)	Δ_a (nm)	MSE rect	MSE trap
0.63 ± 0.03	25.0 ± 0.1	4.0 ± 0.2	5×10^{-3}	3×10^{-3}
0.60 ± 0.03	25.0 ± 0.1	4.4 ± 0.2	5×10^{-3}	3×10^{-3}
0.56 ± 0.04	24.1 ± 0.1	4.6 ± 0.2	3×10^{-3}	2×10^{-3}
0.55 ± 0.01	21.5 ± 0.1	4.4 ± 0.2	4×10^{-3}	3×10^{-3}

^aThe parameter w_0/d is the normalized line width for the chemical patterns. The width of the PS domains is w_r , and the apparent interfacial width is Δ_a . MSE denotes the mean-squared error for the nonlinear regression analysis. Errors are reported for both the rectangular and the trapezoidal models.

calculations, and we speculate the discrepancy is due to contamination on the backside of the nitride membranes.

Acknowledgment. G.E.S acknowledges the NRC-NIST Postdoctoral Fellowship Program for financial support. The Advanced Light Source is supported by the Director, Office of Science, Office of Basic Energy Sciences, of the U.S. Department of Energy under Contract No. DE-AC02-05CH11231. Research was performed in part at the NIST Center for Nanoscale Science and Technology. We thank A. W. Bosse, W. L. Wu, C. Q. Wang, and E. J. Kramer for helpful discussions, J. B. Kortright for providing PS and PMMA optical constants, and S. J. Weigand for SAXS measurements (not shown).

Appendix I

Soft X-ray diffraction is sensitive to the domain shape, because the scattering vectors in the x - z plane change as a function of diffraction angle. This is the principal advantage of SoXRD over traditional small-angle diffraction. The following data illustrate the sensitivity to domain sidewall angle: All block copolymer data are analyzed with the constraint $\phi = 0$, i.e. the cross-section is forced to be rectangular. Table 2 summarizes the line widths and apparent interfacial widths that are calculated with the rectangular model. The mean-squared error for regression analysis with the rectangular and trapezoidal models are compared.

There are three important findings: First, the volume of the PS domain varies with the chemical pattern line width and does not satisfy the 50% volume requirement. Second, the apparent interfacial width drops to approximately 4.3 nm, which is less than expected for an interface broadened by thermal fluctuations, assuming the models and physical parameters used to calculate Δ and $\langle \delta_x^2 \rangle$ are accurate. Third, the mean-squared error from regression analysis is approximately 20% larger when the shape is constrained to a rectangle. Fit results subject to the $\phi = 0$ constraint are shown in Figure 10, and it is clear that the rectangular model does not capture all the diffraction peaks.

Appendix II

The magnitude of line-edge roughness calculated with eq 7 is highly sensitive to estimates for the temperature-dependent PS-PMMA physical constants. The value of χ selected for analysis in the Results and Discussion was calculated by Zhao et al. from small-angle X-ray scattering profiles analyzed with Leibler's mean-field theory.^{25,42} The following paragraphs illustrate how the results are changed if a different reference for χ is used to predict the structure of a block copolymer interface broadened by capillary waves.

An earlier measurement of χ for nondeuterated PS/PMMA systems was based on cloud point measurements from blends (Callaghan et al.), and is $\chi \approx 0.028$ at 240 °C.³¹ The modifies predictions for the PS-PMMA interface structure as follows:

- $\Delta = 4.7$ nm (mean-field interfacial width incorporating chain end effects).

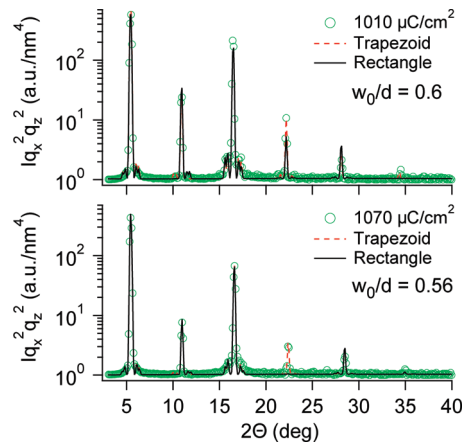


Figure 10. Comparison of rectangular and trapezoid model for analysis of SoXRD data. The rectangle model ($\phi = 0$) cannot fit all the peak amplitudes accurately. This is most clearly observed at the fourth diffraction peak.

Table 3. Comparing the PS-PMMA Interfacial Structure Predicted with the Callaghan and Zhao χ values^a

χ	Δ pred, nm	Δ_a pred, nm	3σ pred, nm	3σ meas, nm
0.028 ³¹	4.7	5.5	3.5	1.7 ± 1.7
0.037 ²⁵	4.0	4.9	3.3	3.3 ± 1.5

^aThe uncertainty in 3σ measurement assumes 5% error in all physical constants.

- $\Delta_a = 5.5$ nm (apparent interfacial width predicted with the capillary wave model).
- $3\sigma_{lr} = 3.5$ nm (low-frequency line-edge roughness).

Our measured value of the apparent interfacial width is (4.9 ± 0.1) nm, which is smaller than expected for the interface broadened by capillary waves with $\chi \approx 0.028$. This finding could be rationalized as follows: First, the epitaxy process pins each domain to the substrate, which could inhibit longer-wavelength fluctuations. Such behavior has been observed in ultrathin homopolymer films confined between two interfaces.³⁴ Second, the different boundary conditions at the substrate interface and film surface likely introduce a z -dependence to the fluctuation spectrum that is not incorporated in this analysis.^{6,43} Third, the capillary wave model may not be appropriate for studying these fluctuations. Monte Carlo simulations suggest that the coupling between neighboring lamellae will produce coherent undulations across multiple domains rather than capillary waves, and while the error associated with using eq 6 to model the resulting interfacial profile is small, it does overestimate the fluctuation contribution to Δ_a by a few tenths of a nanometer.⁴⁴ With these factors in mind, we could estimate the fluctuation-induced low-frequency line-edge roughness for $\chi \approx 0.028$ as follows:

- The mean-field interfacial width is set to 4.7 nm (the value predicted by eq 5).
- The variance in the interface position is calculated from eq 7, i.e. $\langle \delta_x^2 \rangle = (\Delta_a^2 - \Delta^2)/2\pi$, and is approximately $\langle \delta_x^2 \rangle = 0.32$ nm².
- The low frequency ($< 200 \mu\text{m}^{-1}$) line-edge roughness for this PS-PMMA system is then **estimated** as $3\sigma = 3\langle \delta_x^2 \rangle^{0.5} \approx 1.7$ nm. Note that a 5% error in the physical parameters introduces a 0.2 nm uncertainty in calculations of Δ , and the uncertainty in measurements of Δ_a is 0.1 nm (standard deviation). This means 3σ with $\chi \approx 0.028$ could be zero, or as large as 2.4 nm.

The Callaghan et al. χ value for nondeuterated PS/PMMA is less than reported for deuterated copolymers,^{45,46} while the Zhao et al. χ value is larger. Comparisons of deuterated-PS/PMMA

and PS/PMMA interfacial structures (Table 3) demonstrate the latter system has a higher interaction energy,⁴⁷ which supports the use of the larger χ value in our analysis.

Supporting Information Available: Details regarding the patterning and machining of silicon nitride membranes, and PS/PMMA optical constants as a function of photon energy. This material is available free of charge via the Internet at <http://pubs.acs.org>.

References and Notes

- (1) *International technology roadmap for semiconductors*; Technical Report, **2007** (See sections titled Lithography and Emerging Research Materials).
- (2) Stoykovich, M. P.; Kang, H.; Daoulas, K. C.; Liu, G.; Liu, C. C.; de Pablo, J. J.; Mueller, M.; Nealey, P. F. *ACS Nano* **2007**, *1*, 168–175.
- (3) Black, C. T. *ACS Nano* **2007**, *1*, 147–150.
- (4) Kim, S. O.; Solak, H. H.; Stoykovich, M. P.; Ferrier, N. J.; de Pablo, J. J.; Nealey, P. F. *Nature* **2003**, *424*, 411–414.
- (5) Edwards, E. W.; Muller, M.; Stoykovich, M. P.; Solak, H. H.; de Pablo, J. J.; Nealey, P. F. *Macromolecules* **2007**, *40*, 90–96.
- (6) Cheng, J. Y.; Rettner, C. T.; Sanders, D. P.; Kim, H. C.; Hinsberg, W. D. *Adv. Mater.* **2008**, *20*, 3155–3158.
- (7) Villarrubia, J. S.; Vladar, A. E.; Postek, M. T. *Surf. Interface Anal.* **2005**, *37*, 951–958.
- (8) Wang, C.; Araki, T.; Ade, H. *Appl. Phys. Lett.* **2005**, *87*.
- (9) Mitchell, G. E.; Landes, B. G.; Lyons, J.; Kern, B. J.; Devon, M. J.; Koprinarov, I.; Gullikson, E. M.; Kortright, J. B. *Appl. Phys. Lett.* **2006**, *89*.
- (10) Virgili, J. M.; Tao, Y.; Kortright, J. B.; Balsara, N. P.; Segalman, R. A. *Macromolecules* **2007**, *40*, 2092–2099.
- (11) Ade, H.; Hitchcock, A. P. *Polymer* **2008**, *49*, 643–675.
- (12) In a SAXD experiment, the momentum transfer along the z -axis is zero and the scattering pattern is not sensitive to the nanostructure shape. Furthermore, parasitic scattering is observed at low- q , and can be particularly strong when the sample has structure parallel to the beam (such as vertical domain walls).⁴⁸ This is observed in scattering measurements from oxide wells on silicon substrates.
- (13) In this paper, uncertainties are quoted as ± 1 standard deviation unless otherwise noted.
- (14) No defects are detected in SEM measurements, provided the chemical pattern contrast is optimal and uniform across the wafer. This is described in the Experimental Section.
- (15) The scattering volume of the chemical patterns is much smaller than that of the ZEP or PS–PMMA resists, since they are very thin. There is also some topography from the etch. This factors combined make it difficult to measure with transmission SoXRD.
- (16) Perera, G. M.; Stein, G. E.; Liddle, J. A. **2009**. Manuscript in preparation.
- (17) Semenov, A. N. *Macromolecules* **1993**, *26*, 6617–6621.
- (18) Shull, K. R.; Mayes, A. M.; Russell, T. P. *Macromolecules* **1993**, *26*, 3929–3936.
- (19) Semenov, A. N. *Macromolecules* **1994**, *27*, 2732–2735.
- (20) Jones, R. L.; Hu, T.; Lin, E. K.; Wu, W. L.; Kolb, R.; Casa, D. M.; Bolton, P. J.; Barclay, G. G. *Appl. Phys. Lett.* **2003**, *83*, 4059–4061.
- (21) Ruland, W. J. *Appl. Crystallogr.* **1971**, *4*, 70–73.
- (22) Anastasiadis, S. H.; Russell, T. P.; Satija, S. K.; Majkrzak, C. F. *J. Chem. Phys.* **1990**, *92*, 5677–5691.
- (23) Guinier, A. *X-ray diffraction in crystals, imperfect crystals, and amorphous bodies*; Dover Publications, Inc.: London, 1994; It is possible that the pitch does not vary sinusoidally from $d(1 - \epsilon)$ to $d(1 + \epsilon)$, but rather exhibits two discrete values $d(1 \pm \epsilon)$. The latter case would present with higher-order satellite peaks, but they may be too weak to observe.
- (24) A Gaussian resolution function was used with angular divergence $d\theta = 4$ mrad and energy resolution $d\lambda/\lambda \approx 1/2000$.
- (25) Zhao, Y.; Sivaniah, E.; Hashimoto, T. *Macromolecules* **2008**, *41*, 9948–9951.
- (26) Fetters, L. J.; Lohse, D. J.; Richter, D.; Witten, T. A.; Zirkel, A. *Macromolecules* **1994**, *27*, 4639–4647.
- (27) Krishnamoorti, R.; Graessley, W. W.; Zirkel, A.; Richter, D.; Hadjichristidis, N.; Fetters, L. J.; Lohse, D. J. *J. Polym. Sci., Part B: Polym. Phys.* **2002**, *40*, 1768–1776.
- (28) Orofino, T. A.; Ciferri, A. *J. Phys. Chem.* **1964**, *68*, 3136–3141. This reference provides temperature dependence of the poly(styrene) statistical segment length.
- (29) Tsui, O. K. C.; Russell, T. P.; Hawker, C. J. *Macromolecules* **2001**, *34*, 5535–5539. This reference provides the thermal expansion coefficient for PS thin films on a PS brush.
- (30) Wu, W. L.; Vanzanten, J. H.; Orts, W. J. *Macromolecules* **1995**, *28*, 771–774. This reference provides the thermal expansion coefficient for PMMA thin films pinned to a substrate.
- (31) Callaghan, T. A.; Paul, D. R. *Macromolecules* **1993**, *26*, 2439–2450.
- (32) The high-frequency variance $\Delta^2/8$ is estimated from an error function interface concentration profile, rather than the hyperbolic tangent profile.
- (33) Forster, S.; Timmann, A.; Konrad, M.; Schellbach, C.; Meyer, A.; Funari, S. S.; Mulvaney, P.; Knott, R. *J. Phys. Chem. B* **2005**, *109*, 1347–1360.
- (34) Sferazza, M.; Xiao, C.; Jones, R. A. L.; Bucknall, D. G.; Webster, J.; Penfold, J. *Phys. Rev. Lett.* **1997**, *78*, 3693–3696.
- (35) Lacasse, M. D.; Grest, G. S.; Levine, A. J. *Phys. Rev. Lett.* **1998**, *80*, 309–312.
- (36) Wang, Z. G. *J. Chem. Phys.* **1994**, *100*, 2298–2309.
- (37) Kim, S. O.; Kim, B. H.; Kim, K.; Koo, C. M.; Stoykovich, M. P.; Nealey, P. F.; Solak, H. H. *Macromolecules* **2006**, *39*, 5466–5470.
- (38) Wang, C. Q.; Jones, R. L.; Lin, E. K.; Wu, W. L.; Rice, B. J.; Choi, K. W.; Thompson, G.; Weigand, S. J.; Keane, D. T. *J. Appl. Phys.* **2007**, *102*. Coherent undulations are a form of correlated line-edge roughness that produce satellite peaks in the diffraction data. The satellite peaks we observe are associated with noise in the exposure, not undulations, which is clearly demonstrated by comparison of the block copolymer data with measurements from the electron beam resist.¹⁶
- (39) Edwards, E. W.; Montague, M. F.; Solak, H. H.; Hawker, C. J.; Nealey, P. F. *Adv. Mater.* **2004**, *16*, 1315–1318.
- (40) Huang, E.; Rockford, L.; Russell, T. P.; Hawker, C. J. *Nature* **1998**, *395*, 757–758.
- (41) Butler, J. H.; Joy, D. C.; Bradley, G. F.; Krause, S. J. *Polymer* **1995**, *36*, 1781–1790.
- (42) Leibler, L. *Macromolecules* **1980**, *13*, 1602–1617.
- (43) Daoulas, K. C.; Muller, M.; Stoykovich, M. P.; Kang, H.; de Pablo, J. J.; Nealey, P. F. *Langmuir* **2008**, *24*, 1284–1295.
- (44) Geisinger, T.; Muller, M.; Binder, K. *J. Chem. Phys.* **1999**, *111*, 5251–5258.
- (45) Russell, T. P.; Hjelm, R. P.; Seeger, P. A. *Macromolecules* **1990**, *23*, 890–893.
- (46) Russell, T. P. *Macromolecules* **1993**, *26*, 5819.
- (47) Harton, S.; Stevie, F.; Ade, H. *Macromolecules* **2006**, *39*, 1639–1645.
- (48) Stein, G. E.; Lee, W. B.; Fredrickson, G. H.; Kramer, E. J.; Li, X.; Wang, J. *Macromolecules* **2007**, *40*, 5791–5800.